Available online at www.sciencedirect.com
SCIENCE DIRECT®
ELSEVIER
Palaeogeography, Palaeoclimatology, Palaeoecology 236 (2006) 290–301
PALAEO
www.elsevier.com/locate/palaeo

Late Miocene to Pleistocene paleoceanographic records from the Feni and Gardar Drifts: Pliocene reduction in abyssal flow

N.J.C. Hassold [a,*], D.K. Rea [a], B.A. van der Pluijm [a], J.M. Parés [a], J.D. Gleason [a], A.C. Ravelo [b]

[a] *Department of Geological Sciences, University of Michigan, Ann Arbor, MI, USA*
[b] *Ocean Sciences Program, University of California, Santa Cruz, Santa Cruz, CA, USA*

Received 28 January 2004; received in revised form 2 August 2005; accepted 2 November 2005

Abstract

Magnetic fabric analyses from two North Atlantic drift deposits provide proxies for determining relative variations in the strength of abyssal flow over the last 10 my. The data show a cessation of current-controlled sedimentation at the shallower Feni Drift (2417 m) at the time of onset of Northern Hemisphere glaciation (2.6 Ma). Drift formation ended nearly 2 my earlier (4.2 Ma) at the deeper Gardar Drift (3220 m), implying stepwise reduction in deep-water flow. Relatively light $\delta^{18}O$ values at the deeper Gardar Drift indicate a warmer, thus also more salty, water mass site prior to 6 Ma. We interpret this as representing Mediterranean Sea water, which flowed north at depths greater than that of the Feni Drift Site. The supply of Mediterranean Water to the North Atlantic was shut off as the Gibraltar Straits closed, causing the Messinian salinity crisis, and never returned to that position in the water column after the Mediterranean opened again.

Keywords: DSDP Sites 610 and 611; North Atlantic; Drift deposits; Magnetic fabric; Paleoceanography

1. Introduction

Global climate is greatly influenced by ocean circulation, especially the formation of cold, deep water at high latitudes and the concomitant movement of warm surface water away from the equator; this has been called the ocean "conveyor" (Broecker, 1991;Wold, 1994; Jansen and Raymo, 1996; Hansen et al., 2004). In the North Atlantic, the Gulf Stream brings warm, saline water to the Norwegian–Greenland Sea, where these waters cool and sink, forming the North Atlantic Deep Water (NADW) (Howe et al., 1994; Wold, 1994). Over geologic time, the deepening of the Icelandic gateways has controlled this formation of NADW, specifically the subsidence of the Greenland–Iceland–Scotland Ridge (Jansen and Raymo, 1996; Wright and Miller, 1996). Here, waters flowing south from the Norwegian Sea divide: one branch flows over the Iceland–Faeroe Ridge and enters the Iceland Basin; the other branch flows over the Wyville-Thompson Ridge, enters the Rockall Trough, flows around the Rockall-Hatton Bank and then into the Iceland Basin (Fig. 1). In the Iceland Basin, this water mixes with water from the flow over the Iceland–Faeroe Ridge, flows along the Reykjanes Ridge through the Charlie-Gibbs Fracture Zone and into the western North Atlantic (Fig. 1).

* Corresponding author.
E-mail address: nhassold@umich.edu (N.J.C. Hassold).

0031-0182/$ - see front matter © 2005 Elsevier B.V. All rights reserved.
doi:10.1016/j.palaeo.2005.11.011

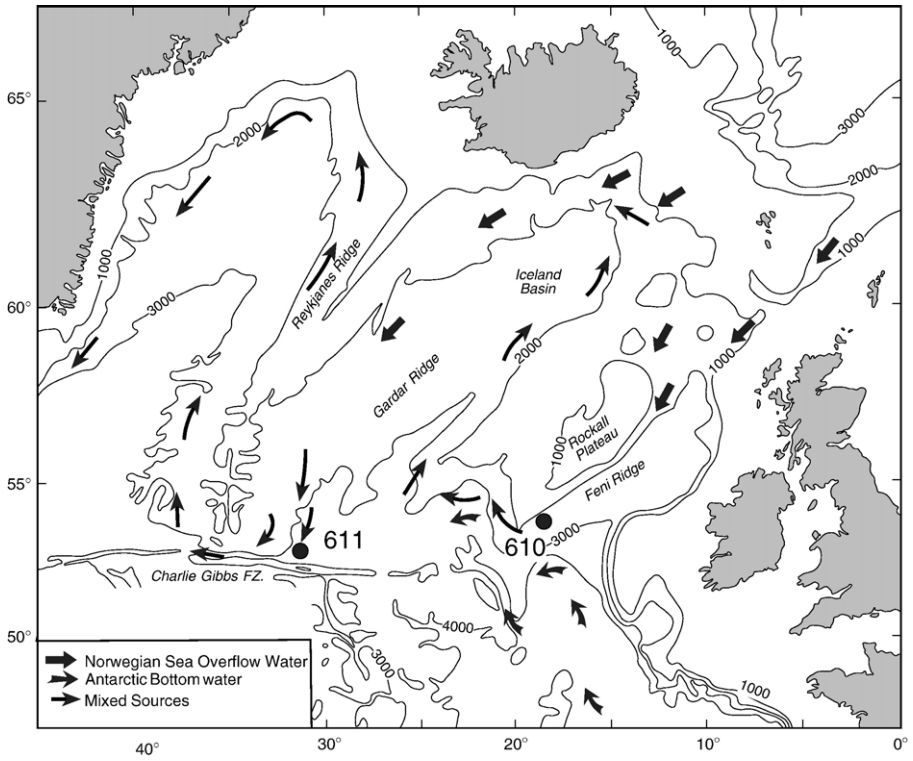

Fig. 1. Location of DSDP Leg 94 Sites 610 (Feni Drift, 2417m depth) and 611 (Gardar Drift, 3220 m depth) (after Kidd and Hill, 1987). Depths shown in meters.

These flows move along the seafloor where they entrain and transport sediment, commonly depositing them parallel to the deep-sea topography when the current velocity decreases, forming drift deposits. Drift deposits are hundreds of kilometers in length, relatively narrow, may have wave-like bed forms and are associated with strong deep-sea currents (Wold, 1994; ODP, Shipboard Scientific Party, 1998).

Drift deposits contain physical and sedimentological records of their depositional history. Using anisotropy of magnetic susceptibility (AMS) and particle size analysis, Ellwood and Ledbetter (1977, 1979) and Ellwood et al. (1979) studied past current flow velocities in the Vema Channel. In general, they determined a direct relationship between the magnetic fabric strength, AMS, grain size and current velocity; stronger fabric and coarser grain size were indicative of higher current velocity.

Joseph et al. (1998) combined the use of magnetic fabric analysis and grain size distribution to estimate depositional energy fields for samples from the Blake Outer Ridge and the Bermuda Rise sediment drifts and the Delgada Deep Sea Fan offshore from northern California. They found that the combination of magnetic fabric and grain-size distribution define specific sediment depositional fields—eolian, hemipelagic mud, drift deposits and turbidites. The magnetic fabric strength is a measure of grain alignment; in samples where the sediment grains are randomly oriented, there is no fabric. Abyssal flow aligns the grains; the strength of the current influences the median grain size and the grain-size distribution in addition to the strength of the magnetic fabric (Rea and Hovan, 1995; Joseph et al., 1998). These methods have successfully been applied to studies of drift deposits on the Kerguelen Plateau in the southern Indian Ocean (Joseph et al., 2002) and the Campbell Plateau, east of New Zealand (Joseph et al., 2004).

Here we present a reconnaissance study of drift deposits in the North Atlantic that spans late Miocene to Pleistocene time, a period that encompasses much of the late Cenozoic global cooling. In addition to sediment composition, mass accumulation rate and stable isotopic signatures of benthic foraminifera, we determined the magnetic fabric of the bulk sediment. The radiogenic isotope geochemistry of terrigenous grains extracted from a few samples provides an indication of their provenance. These data were obtained with the goal of examining the general history of late Cenozoic abyssal flow in the North Atlantic.

1.1. Geologic setting and samples

Sites occupied during Leg 94 of the Deep Sea Drilling Project (DSDP) were usually located on drift deposits (Fig. 1). The Feni Drift lies where Norwegian Sea Overflow Water (NSOW) flows over the Wyville-Thompson Ridge and down through the Rockall Trough. The Gardar Drift is a large (1000 km long) drift deposit located along the lower eastern flank of the Reykjanes Ridge, where water from the Iceland Basin flows south toward the Charlie-Gibbs Fracture Zone and on into the western Atlantic Basin. Both drifts have large-scale wave-like bedforms, but Hailwood et al. (1987) and Kidd and Hill (1987) found no consistent link between these wave fields and present bottom water flow. They concluded that the sediment waves are relict features that migrated during the late Pliocene, due to a more vigorous NSOW, but that the migration ceased at the Plio/Pleistocene boundary and ensuing pelagic sediments drape the sediment waves.

For this reconnaissance investigation of the North Atlantic drifts, 38 separate sample pairs (adjacent sediment scoop samples and paleomagnetic cube samples), 17 from the Feni Drift and 21 from the Gardar Drift, were obtained from cores recovered at DSDP Sites 610 and 611. Site 610 was drilled on the southern end of the Feni Drift (53°13.5′N, 18°53.7′W, 2417 m water depth) and recovered nannofossil ooze and chalk. Accumulation of sediments at the Feni Drift is believed to have started around the time of the Eocene–Oligocene boundary (Kidd and Hill, 1987; Jansen and Raymo, 1996); the oldest sediment recovered at Site 610 was late early Miocene in age (Ruddiman et al., 1987a; Howe et al., 1994; Wold, 1994). Site 611 was drilled in the trough of a sediment wave at the southern end of the Gardar Drift (52°50.5′N, 30°18.6′W, 3220 m water depth) and recovered marly nannofossil chalk. Accumulation on the Gardar Drift began in the middle to early–late Miocene; the oldest sediments recovered at this site are late Miocene in age (Ruddiman et al., 1987b; Wold, 1994; Jansen and Raymo, 1996). For this study, we sampled cores from Holes 610, 610A and 611C.

2. Methods

2.1. Age and age models

Ages were determined by magnetic reversal stratigraphy for all of the sediments from Hole 611C and for sediments younger than 8 Ma for Hole 610 using the 1995 Cande and Kent timescale (Cande and Kent, 1995). Approximate biostratigraphic ages for the four oldest samples from Hole 610 were determined using the nannofossil zones as given by Takayama and Sato (1987) and referring to the Berggren et al. (1995) timescale (Fig. 2). Fluxes were calculated using the linear sedimentation rate (LSR) as shown on Fig. 2 and the dry bulk density (DBD) data for each site taken from the Leg 94 Initial Reports (Ruddiman et al., 1987a; Ruddiman et al., 1987b). Mass accumulation rates (MAR) of the sediment components were calculated using the % terrigenous component or % $CaCO_3$ and the flux (MAR component = LSR × DBD × % component). These data are summarized in Tables 1 and 2.

2.2. Carbonate fraction determination

Carbonate concentrations of the bulk sample were determined by measuring the volume of CO_2 released when each sample was treated with 3 N HCl–the carbonate bomb method–as described by Müller and Gastner (1971). The resulting percentages are accurate to ± 1 wt.% (Tables 1 and 2).

2.3. Terrigenous fraction determination

Sediment samples were freeze-dried and the terrigenous component was isolated using the chemical extraction method described by Rea and Janecek (1981) as modified by Hovan (1995), which removes carbonates, oxides and hydroxides and biogenic silica. Weight percent terrigenous component data are accurate to ± 2% to 3% of the values (Tables 1 and 2).

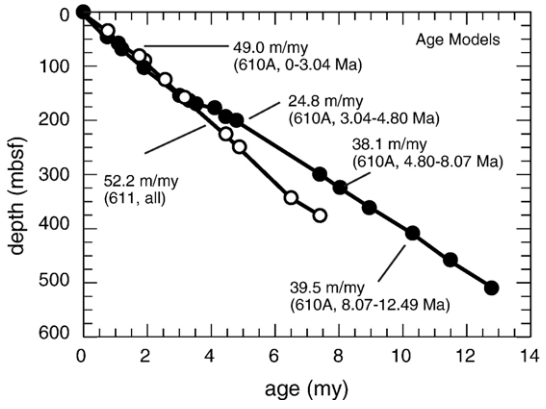

Fig. 2. Age models and linear sedimentation rates for Sites 610 and 611. Ages for sediments from Hole 611C and sediments younger than 8 Ma for Hole 610 were determined using the 1995 Cande and Kent timescale (Cande and Kent, 1995). Approximate biostratigraphic ages for the four oldest samples from Hole 610 were determined using the nannofossil zones as given by Takayama and Sato (1987) and referring to the Berggren et al. (1995) timescale.

Table 1
Data for Feni Drift Site 610

Sample # hole-core section	Depth (mbsf)	Age (Ma)	Granisize (Φ_{50})	Granisize (μm)	% $CaCO_3$	% terrigenous component	MAR (g/cm^2/ky)	$CaCO_3$ MAR (g/cm^2/ky)	Terrigenous MAR (g/cm^2/ky)	P'	T	Bulk susc. ($\times 10^{-6}$ SI)	$\delta^{13}C$ (‰)	$\delta^{18}C$ (‰)
610A-1-3	4.16	0.087	6.4	11.84	43.4	33.1	5.19	2.25	1.72	1.015	0.139	277	0.91	3.83
610A-3-2	20.47	0.426	7.14	7.09	74.5	10.4	5.19	3.87	0.54	1.024	0.048	134		
610A-5-3	41.5	0.865	6.38	12.01	28.6	46.4	5.19	1.49	2.41	0.037	0.668	608	0.50	3.83
610A-7-3	61.3	1.277	6.44	11.52	61.3	18.2	5.19	3.19	0.94	1.021	0.126	208	1.02	2.78
610A-9-3	80.04	1.668	6.33	12.43	78.1	8.4	5.19	4.06	0.43	1.034	−0.048	99	1.17	2.99
610A-11-3	98.78	2.058	5.62	20.33	80.2	6.3	5.19	4.17	0.33	1.046	−0.149	66		
610A-13-3	118.44	2.468	6.71	9.55	76.8	8.5	5.19	3.99	0.44	1.021	−0.029	152	0.23	2.57
610A-15-3	137.64	2.868	6.35	12.26	82.2	7.5	5.19	4.27	0.39	1.332	−0.206	10		
610A-17-3	156.1	3.198	6.23	13.32	93.3	2.5	2.63	2.45	0.07	1.448	0.392	−8	0.41	2.32
610A-19-3	175.86	3.995	5.94	16.29	93.1	2.5	2.63	2.45	0.07	1.275	0.384	−12	1.08	2.43
610A-21-3	194.58	4.750	6.91	8.32	92.8	3.4	2.63	2.44	0.09	1.258	0.372	−13	0.74	2.19
610-10-3	237.22	5.839	6.08	14.78	97.1	3.0	4.04	3.92	0.12	1.257	0.435	−13	0.83	2.19
610-11-2	302.16	7.544	5.3	25.38	95.3	2.3	4.04	3.85	0.09	1.296	0.344	−11	0.97	2.14
610-13-1	359.06	9.037	6.33	12.43	89.9	3.4	4.19	3.76	0.14	2.175	0.486	−4	0.97	2.13
610-14-2	408.32	10.330	5.71	19.10	94.5	13.7	4.19	3.96	0.57	1.355	0.311	−9	1.24	1.77
610-15-3	458	11.634	6.86	8.61	92.6	2.0	4.19	3.88	0.08	1.292	0.331	−11	1.07	1.98
610-16-4	507.87	12.943	6.34	12.34	93.4	6.1	4.19	3.91	0.26	1.409	0.263	−9	1.24	1.80

Table 2
Data for Gardar Drift Site 611

Sample # hole-core section	Depth (mbsf)	Age (Ma)	Granisize (Φ_{50})	Granisize (μm)	% $CaCO_3$	% terrigenous component	MAR ($g/cm^2/ky$)	$CaCO_3$ MAR ($g/cm^2/ky$)	Terrigenous MAR ($g/cm^2/ky$)	P'	T	Bulk susc. ($\times 10^{-6}$ SI)	$\delta^{13}C$ (‰)	$\delta^{18}C$ (‰)
611C-2-2	4.44	0.085	5.7	19.24	74.4	5.8	3.46	2.57	0.20	1.013	0.667	293	0.709	2.757
611C-4-2	14.46	0.277	5.85	17.34	68.1	6.8	3.46	2.35	0.23	1.011	−0.244	423	0.785	3.566
611C-6-2	33.96	0.651	5.88	16.98	54.7	22.7	3.46	1.89	0.78	1.009	0.751	606	0.534	3.295
611C-8-2	53.12	1.018	6.75	9.29	64.4	15.7	3.46	2.23	0.54	1.015	0.651	1007	0.707	27.65
611C-10-2	72.32	1.385	6.68	9.75	55.0	17.6	3.46	1.90	0.61	1.004	−0.236	1282	1.163	29.40
611C-12-2	91.87	1.760	6.52	10.90	53.2	18.1	3.46	1.84	0.62	1.009	−0.256	877		
611C-14-2	110.7	2.121	5.7	19.24	48.8	24.5	3.46	1.69	0.85	1.007	0.037	962		
611C-16-2	129.94	2.489	6.22	13.42	15.3	32.5	3.46	0.53	1.12	1.008	0.525	1281		
611C-18-2	149.68	2.867	6.52	10.90	68.7	8.6	3.46	2.38	0.30	1.011	−0.048	316	0.033	2.434
611C-20-2	168.24	3.223	6.1	14.58	85.7	5.9	3.46	2.96	0.20	1.025	0.112	185	0.793	2.310
611C-22-2	187	3.582	6.82	8.85	77.0	8.8	3.46	2.66	0.30	1.011	−0.434	305	0.765	2.497
611C-24-2	207.08	3.967	7.07	7.44	68.0	9.1	3.46	2.35	0.31	1.011	0.128	509	−0.926	2.607
611C-26-2	225.34	4.317	7.7	4.81	92.1	1.1	3.46	3.18	0.04	1.086	−0.210	37	0.918	2.367
611C-28-2	244.57	4.685	6.8	8.97	84.4	4.6	3.46	2.92	0.16	1.034	−0.101	97	0.507	2.065
611C-30-3	266.19	5.099	5.58	20.91	87.8	2.9	3.46	3.03	0.10	1.187	−0.371	16	0.881	2.020
611C-32-1	282.39	5.410	6.85	8.67	88.5	3.4	3.46	3.06	0.12	1.083	−0.213	35	0.384	2.069
611C-35-1	311.14	5.961	6.19	13.70	83.5	5.4	3.46	2.87	0.19	1.061	0.089	64	0.908	2.142
611C-36-1	320.07	6.132	6.03	15.30	75.2	8.7	3.46	2.60	0.30	1.036	0.042	104		
611C-38-2	341.63	6.545	5.8	17.95	84.4	5.4	3.46	2.92	0.19	1.137	−0.297	22	0.837	1.526
611C-40-1	358.83	6.874	6.82	8.85	75.0	8.4	3.46	2.59	0.29	1.107	−0.153	29	0.520	1.316
611C-42-1	377.76	7.237	6.37	12.09	76.8	16.0	3.46	2.65	0.55	1.107	−0.143	28	0.838	1.048

Table 3
Results from radiogenic isotope analyses for selected sediment samples

Sample	Depth (mbsf)	Age (Ma)	$^{143}Nd/^{144}Nd$[a]	2−σ	ε_{Nd}[b]	$^{87}Sr/^{86}Sr$[c]	2−σ
610A-1-3	4.16	0.08	0.512005	±0.000012	−12.3	0.724321	±0.000018
610A-7-3	61.30	1.18	0.512097	±0.000011	−10.6	0.720435	±0.000017
611C-12-2	91.87	1.93	0.512553	±0.000012	−1.7	0.708139	±0.000017
611C-14-2	110.70	2.29	0.512646	±0.000010	+0.2	0.707196	±0.000015

[a] $^{143}Nd/^{144}Nd$ normalized to $^{146}Nd/^{144}Nd = 0.7219$ (2σ errors represent in-run precision by TIMS on 150 ratios).
[b] $\varepsilon_{Nd} = 10^4[(^{143}Nd/^{144}Nd_{(measured)})/(^{143}Nd/^{144}Nd_{(bulk\ earth)}) - 1]$, where $^{143}Nd/^{144}Nd_{(bulk\ earth)} = 0.512638$.
[c] $^{87}Sr/^{86}Sr$ normalized to $^{86}Sr/^{88}Sr = 0.1194$ (2σ errors represent in-run precision by TIMS on 150 ratios).

2.4. Radiogenic isotope analysis

Four samples of the extracted terrigenous sediment component (two from the Feni Drift and two from the Gardar Drift) were analyzed for radiogenic isotope geochemistry with the goal of constraining provenance (Table 3, Fig. 3). Samples were digested in screw-top Savillex beakers on hot plates using a combination of HF-HNO_3, $HClO_4$ and HCl. Rare earth elements (REE) were separated by conventional cation exchange in HCl medium followed by reverse phase (HDEHP) chromatography to separate Nd and Sm. Sr was separated on a strontium-specific crown ether resin (Sr-Spec) on miniaturized columns. Isotopic ratios were determined at the University of Michigan on a Finnigan 262 Thermal Ionization Mass Spectrometer equipped with eight collectors using static mode. The La Jolla Nd and NBS 987 Sr standards gave mean values of $^{143}Nd/^{144}Nd = 0.511849 \pm 0.000008$ ($N = 17$) and $^{87}Sr/^{86}Sr = 0.710250 \pm 000014$ ($N = 74$) over the course of this study, requiring no corrections to the data (Gleason et al., 2002).

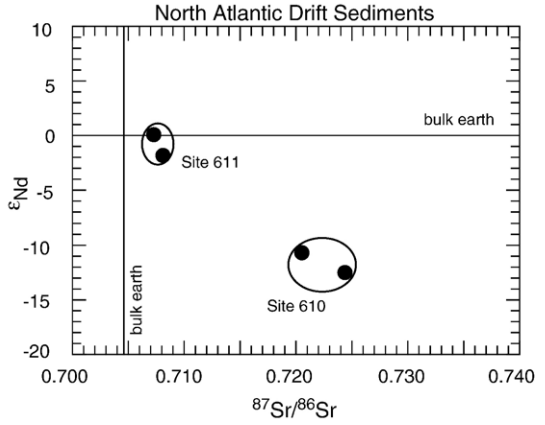

Fig. 3. Radiogenic isotope values for selected samples of terrigenous sediment from Sites 610 and 611. Values for Site 611 are indicative of young oceanic crust, while those for Site 610 are indicative of older continental crust.

2.5. Stable isotope analysis

Oxygen and carbon isotope analyses of foraminifera were determined at the University of California, Santa Cruz, light stable isotope facility on a Prism mass spectrometer with an on-line automated common acid carbonate reaction device (Tables 1 and 2). Analyses were conducted on benthic foraminiferal tests of *Cibicides*, picked individually from each sample and ultrasonically cleaned and dried. External precision on an in-house standard (Carrera Marble) and on NBS carbonate standards is ± 0.05% for $\delta^{13}C$ and ± 0.07% for $\delta^{18}O$.

2.6. Magnetic analyses

Samples from the DSDP cores contained in plastic paleomagnetic sampling cubes were measured on a KLY-2 Kappa Bridge at the University of Michigan to determine the bulk magnetic susceptibility and the P' and T parameters of the susceptibility ellipsoid (Tables 1 and 2). These latter values denote the anisotropy of magnetic susceptibility or magnetic fabric of a sample. Grains that settle through the water column under no influence from current are randomly oriented in the depositional plane, while those deposited under the influence of a current show a preferred orientation or fabric (Ellwood and Ledbetter, 1977, 1979; Joseph et al., 1998). P' is magnitude of the anisotropy of the sample and describes the strength of the magnetic fabric. T is the shape parameter of the susceptibility ellipsoid: when $0 < T < 1$, the ellipsoid is oblate (disk-shaped), if $-1 < T < 0$, it is prolate (cigar-shaped) (Tarling and Hrouda, 1993; Joseph et al., 1998, 2002).

3. Sedimentary record of the Feni and Gardar Drifts

3.1. Site 610: late Cenozoic changes in the Feni Drift

Feni Drift sediment is calcareous ooze, 80–96% $CaCO_3$, with the remainder being terrigenous mineral grains (Fig. 4). ε_{Nd} and $^{87}Sr/^{86}Sr$ values of these mineral

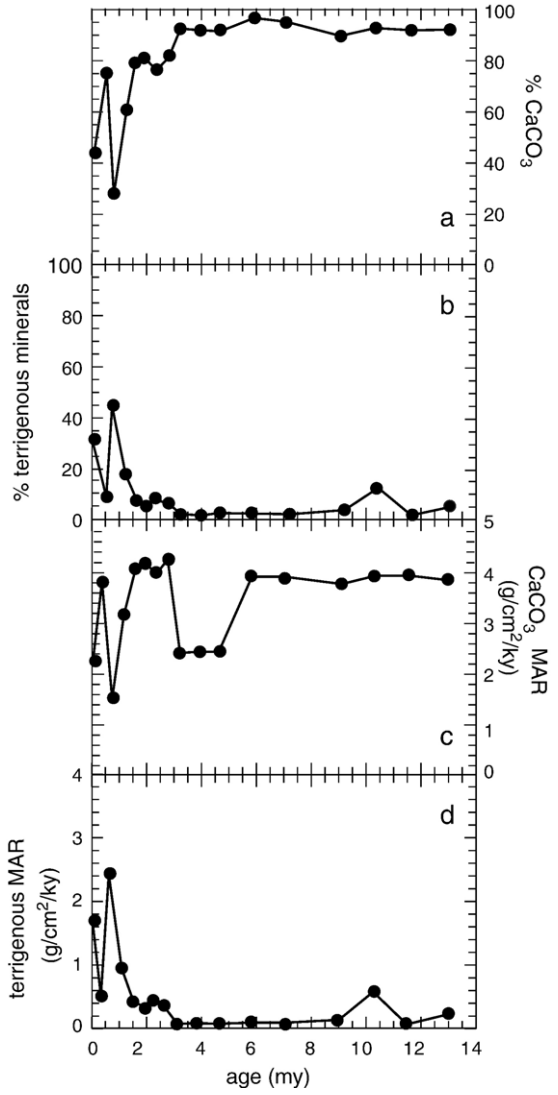

Fig. 4. Weight percent and mass accumulation rates of $CaCO_3$ (a and c) and terrigenous (b and d) components at Site 610 (Feni Drift). The $CaCO_3$ MAR decrease at 5 Ma reflects a lower sedimentation rate at that time. The increase in the terrigenous MAR at 2.6 Ma corresponds to the onset of Northern Hemisphere glaciation.

grains indicate an older (continental) sediment source for Feni Drift, supporting the suggestion of Latouche et al. (1987) and Kidd and Hill (1987) (Fig. 3 and Table 3).

Terrigenous and carbonate sediment fluxes provide the history of sedimentation. An increase in the percent terrigenous component and the bulk susceptibility is seen at 2.6 Ma and 1.2 Ma (Figs. 4 and 5) and is reflected in the terrigenous MAR (Fig. 4). Prior to 6 Ma, the $CaCO_3$ MAR remained fairly constant at ~ 4 g/cm^2/ky (Fig. 4). At 6 Ma, there was a sharp decrease to less than 3 g/cm^2/ky, corresponding to the lower sedimentation rate during this time. For sediments younger than 3 Ma, the sedimentation rate increased with a corresponding increase in the average $CaCO_3$ MAR, until ~ 2 Ma. The average terrigenous MAR was very low prior to 2.6 Ma, then increased at 2.6 Ma and then again by a factor of 6 in the Pleistocene.

A pronounced magnetic fabric characterizes Feni Drift sediment older than 2.6 Ma (Fig. 5). Younger sediments have only a very weak fabric. The P' values recorded here are noticeably greater than those we measured at the Gardar Drift (see below), at the Kerguelen Drift (Joseph et al., 2002) or the Antarctic Peninsula drifts (Rea et al., 2003), all of which were in the range of 1.05 to 1.20.

$\delta^{18}O$ values of benthic foraminifera from the Feni Drift gradually increased (became heavier) beginning about 3 Ma, in the late Pliocene. $\delta^{13}C$ values became lighter in the younger sediments with large variations (1‰) in the Plio/Pleistocene (Fig. 6).

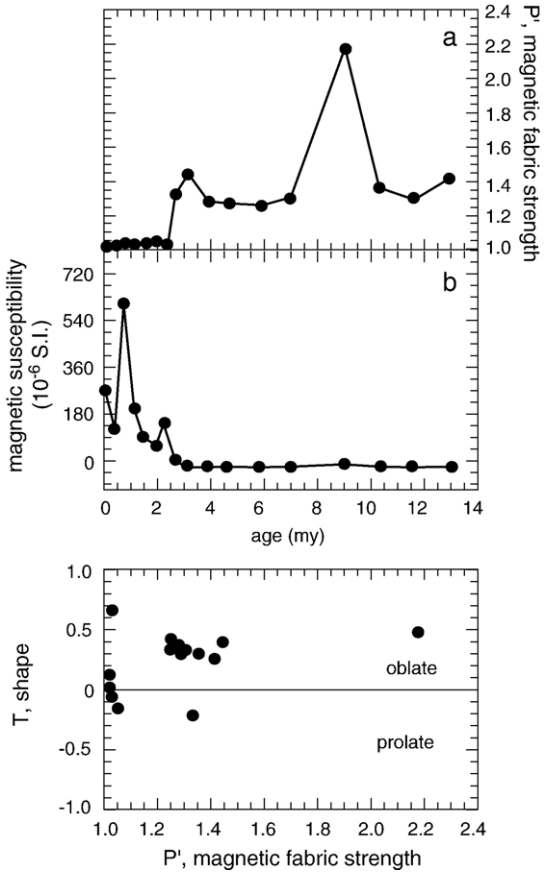

Fig. 5. Magnetic characteristics of samples from Site 610 (Feni Drift). P' (upper panel, a), bulk susceptibility (upper panel, b) and P' vs. T (lower panel). The decrease in magnetic fabric strength, P', indicates a reduction in current strength. The increase in bulk susceptibility reflects the increase in terrigenous component. The T vs. P' plot shows the general shape of the magnetic tensor.

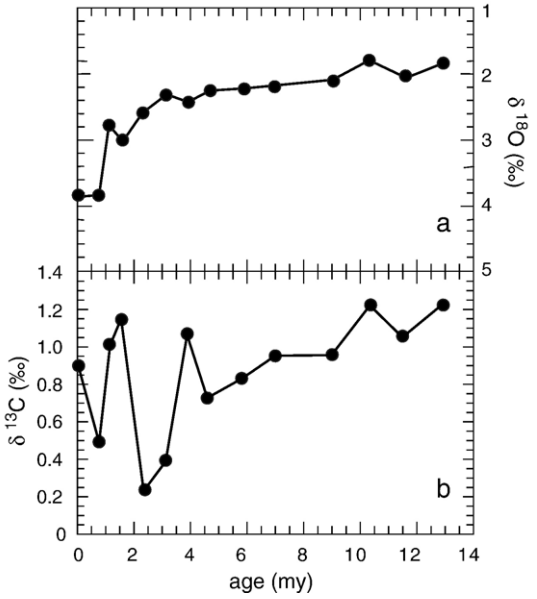

Fig. 6. $\delta^{18}O$ (a) and $\delta^{13}C$ (b) data for Site 610 (Feni Drift). The $\delta^{18}O$ values gradually increase beginning around 3 Ma.

3.2. Site 611: late Cenozoic changes in the Gardar Drift

Sediments from the Gardar Drift are also calcareous ooze with 80–96% $CaCO_3$ and the remainder being terrigenous material (Fig. 7). Results of the ε_{Nd} and $^{87}Sr/^{86}Sr$ analyses of the terrigenous component indicate a younger (basaltic) sediment source for the terrigenous minerals in the Gardar Drift (Fig. 3 and Table 3). Bulk susceptibility (Fig. 8) and terrigenous abundance were low during the late Miocene and early Pliocene and increased at 4.5 Ma and 2.6 Ma (Fig. 7). The $CaCO_3$ MAR was around 2.7 g/cm^2/ky and declined between 4.5 and 2.6 Ma to ~ 2 g/cm^2/ky (Fig. 7). Terrigenous MAR increased slightly at 4.5 Ma and again at 2.6 Ma (Fig. 7).

The magnetic fabric is strong before the early Pliocene but shows a sharp reduction to low values beginning about 5.2 Ma, with very low values younger that 4.2 Ma (Fig. 8). The values prior to 4.2 Ma are comparable to those obtained by Joseph et al. (2002) at ODP Site 745 in the southern Indian Ocean.

At the Gardar Drift, which is the deeper site, $\delta^{18}O$ values are similar to those at shallower Site 610 in sediment younger than about 6 Ma. Older samples show distinctly lighter values for $\delta^{18}O$ (Fig. 9). $\delta^{13}C$ values are generally around 0.5‰ with the exception of one pronounced negative value of − 1.0‰ at 4.1 Ma (Fig. 9).

3.3. Paleoceanography of the North Atlantic drifts

Both sites show changes in the terrigenous and carbonate fluxes that occurred around 2.6 Ma, corresponding to the onset of Northern Hemisphere glaciation. At the Feni Drift, the terrigenous MAR increase was several-fold (Fig. 4d); the result of increased continental glacial erosion as evidenced by the geochemistry of the terrigenous grains. The carbonate flux gradually declined during the late Miocene through the mid-Pliocene. The sharp decrease to lower carbonate MAR values at 5 Ma mirrors a decrease in overall sedimentation rate, which later increased to higher values between 3 Ma and 1 Ma (Fig. 4c).

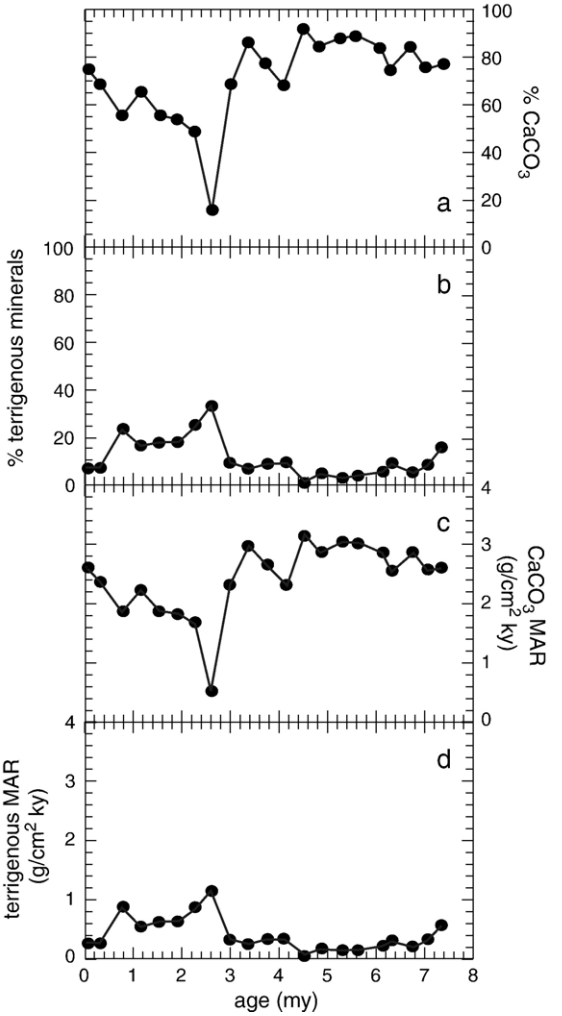

Fig. 7. Weight percent and mass accumulation rates of $CaCO_3$ (a and c) and terrigenous (b and d) components at Site 611 (Gardar Drift). The $CaCO_3$ MAR decrease occurs around 2 Ma (the very low point around 2.5 Ma is an outlier). The terrigenous MAR increases slightly at 4 Ma and then again at 3 Ma.

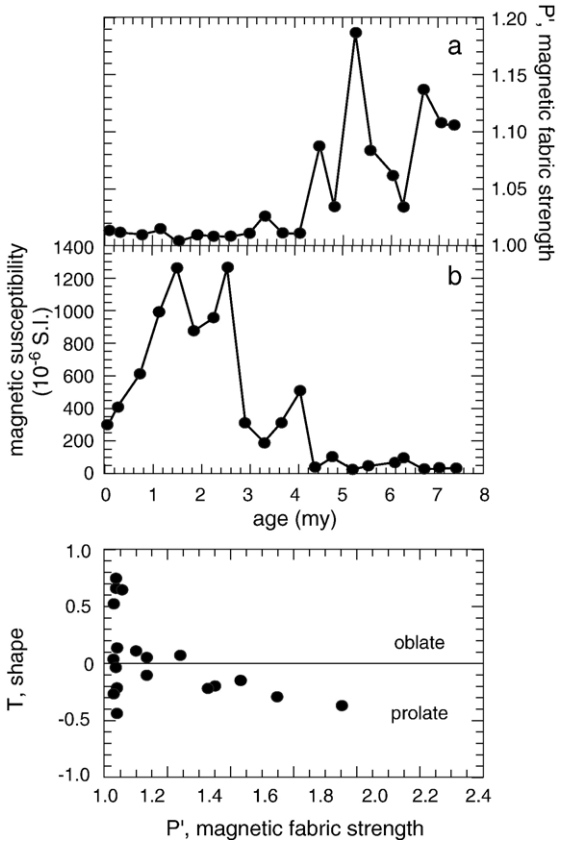

Fig. 8. Magnetic characteristics of samples from Site 611 (Gardar Drift). P' (upper panel, a), bulk susceptibility (upper panel, b) and P' vs. T (lower panel). The decrease in magnetic fabric strength, P', at 5 Ma indicates a reduction in current strength. The increase in bulk susceptibility at 5 Ma reflects the increase in terrigenous component. The T vs. P' plot shows the general shape of the magnetic tensor.

At the Gardar Drift, the terrigenous MAR (Fig. 7d) increased in two steps beginning around 4.5 Ma and again at 2.6 Ma. An increase in ice rafted debris from southeastern Greenland around 4 Ma (St. John and Krissek, 2002) implies glaciers at sea level prior to the onset of full scale Northern Hemisphere glaciation at 2.6 Ma, although Greenland is unlikely to be the source of fine-silt sized terrigenous grains at Site 611. There was also a terrigenous MAR increase at the onset of Northern Hemisphere glaciation at the Gardar Drift and the geochemistry of these materials implicate Iceland as a possible source (Fig. 3). Carbonate fluxes at Site 611 decreased rapidly between 4.5 Ma and 3 Ma and remained somewhat lower until the present (Fig. 7c).

At the Feni Drift Site (2417 m), the magnetic fabric strength was strong prior to the late Pliocene (Fig. 5a). Between 3.2 and 2.5 Ma, the fabric strength fell to very low values and has remained low to the present. We interpret this decrease as marking a reduction in current flow at this time, an end to drift deposition and a concomitant large decrease in the export of cold water from high latitudes. This interpretation is in agreement with histories of North Atlantic Deep Water formation based upon $\delta^{13}C$ analyses of benthic foraminifera. Studies of sites at water depths similar to that of DSDP 610 show a strong NADW flux approximately 3 my ago, followed by a pronounced weakening of that flow with the onset of Northern Hemisphere glaciation (Raymo et al., 1992; Ravelo and Andreasen, 2000).

Magnetic fabric strength at the Gardar Drift Site (3220 m) was moderate in the late Miocene to the early Pliocene but declined to low values between 5.2 Ma and 4.2 Ma (Fig. 8a). Similar to the Feni Drift, this decrease implies a decrease in current flow and an end to drift deposition, but occurs almost 2 my earlier. These data show that deep (~ 3220 m) water flow slowed or stopped before more shallow (~ 2417 m) flow did, implying a complex, stepwise reduction in bottom flow during the Pliocene. This evidence for early Pliocene flow reduction was not an anticipated result of our research, but it agrees with the results obtained from the DSDP Leg 94 (Kidd and Hill, 1987).

Prior to 6 Ma, the Gardar Drift sediments had a much lighter benthic $\delta^{18}O$ signal than the Feni Drift (Fig. 10). Since Site 611 is the deeper of the two (3220

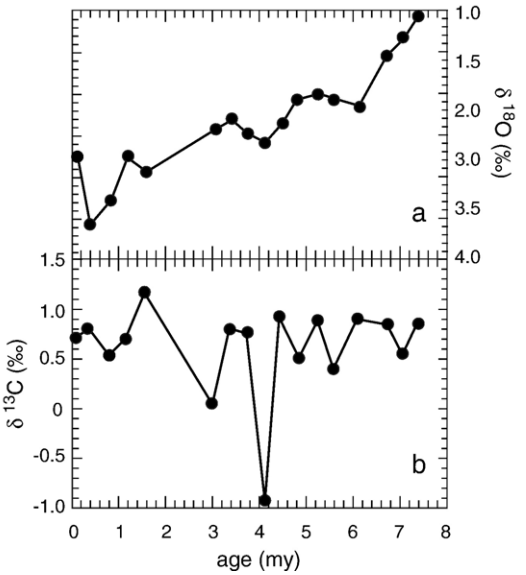

Fig. 9. $\delta^{18}O$ (a) and $\delta^{13}C$ (b) data for Site 611 (Gardar Drift). The $\delta^{18}O$ values increase steadily. The increase between 6 and 8 Ma is interpreted to indicate a decrease in Mediterranean water input due to the Messinian salinity crisis.

m), density considerations indicate a water mass that is both warmer and more saline. This shift in isotopic values was also seen at deeper Site 608 (3526 m), but is less than half as large there (~ 0.5‰ at 608) (Wright and Miller, 1996); no similar late Miocene change in $\delta^{18}O$ occurred at Site 610 (2417 m) (Fig. 10). The suggestion of a different water mass before 6 Ma at Site 611 is consistent with the results of Murray (1987) and of Thomas (1987) who analyzed benthic foraminifera assemblages and inferred a latest Miocene change in the nature of the water masses at Site 611. We interpret the light $\delta^{18}O$ values prior to 6 Ma at Site 611 as indicating warm, salty Mediterranean-origin water that flowed out into the Atlantic and north at a depth greater than 2417 m (the depth of Feni Drift). Zhang and Scott (1996), in an extensive stratigraphic study, have documented the presence of paleo-Mediterranean outflow water in the North Atlantic prior to the end of the Miocene. Our data suggest that the main core of this water mass was below 2417 m and closer to 3220 m (Gardar Drift) than 3526 m (Site 608). The closing of the Straits of Gibraltar, which precipitated the Messinian salinity crisis (Hsü et al., 1973; Krijgsman et al., 1999; Seidenkrantz et al., 2000; Duggen et al., 2003), would have terminated this outflow just after 6 Ma. Since the reopening of the Straits of Gibraltar, Mediterranean water flows north along the continental margin of Europe and shoals in the Norwegian Sea, where it is incorporated into the NADW (Reid, 1979).

Carbon isotope values ($\delta^{13}C$) for both Sites 611 and 610 correspond well for samples younger than about 5 Ma (Fig. 11). Prior to this, the water mass at Site 611 appeared lighter (older) than at Site 610. There is a large single-point negative value at Site 611, possibly

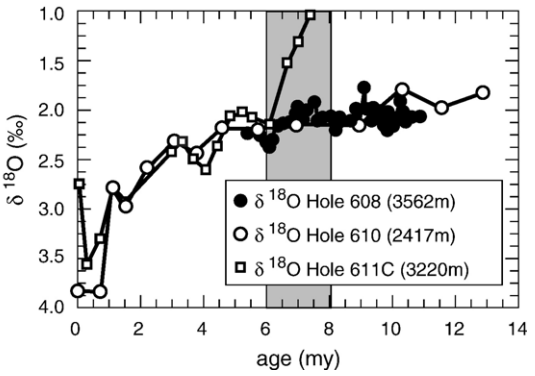

Fig. 10. Oxygen isotope comparison among Holes 608, 610 and 611C. The values for all three holes track well after 6 Ma. Prior to 6 Ma, values from Hole 611C indicate a warmer, more saline water mass, probably Mediterranean water.

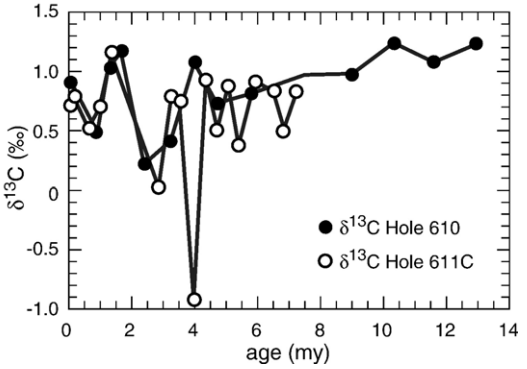

Fig. 11. Comparison of $\delta^{13}C$ values between Hole 610 (Feni Drift) and Hole 611C (Gardar Drift). The reason for the large negative value at 4 Ma for Hole 611C is not known, but the value is probably real. Other researchers have noted a similar excursion at other sites.

the same as seen by Billups (2002), but the cause of this apparently brief event is not known.

4. Conclusions

Our study of the Feni and Gardar Drifts provides the following insights into North Atlantic paleoceanography. Whereas many of our observations amplify the work of previous investigators (Kidd and Hill, 1987; Raymo et al., 1992; Zhang and Scott, 1996; Krijgsman et al., 1999; Frank et al., 2002; Laberg et al., 2005), the temporal details of the reductions in deep water outflow from the region are new. Prior to approximately 6 Ma, warm salty water from the Mediterranean occupied mid depths, constrained to between 2400 and 3600 m, in the North Atlantic. During these late Miocene times, the Feni and Gardar Drifts were being deposited by deep currents, with the flow at the shallower Feni Drift site being relatively stronger than that at the deeper Gardar Drift site. The gradual closing of the Straits of Gibraltar at the end of the Miocene precipitated the Messinian salinity crisis in the Mediterranean basin and shut off the supply of Mediterranean overflow water to the North Atlantic (as indicated by the $\delta^{18}O$ data).

Krijgsman et al. (1999) note that the Mediterranean became isolated from the North Atlantic between about 5.6 and 5.3 million years ago. Shortly after this time, the deeper Gardar drift current began to slow and the flow was nearly completely gone by 4.2 Ma. We suggest that, without the salt supplied by the Mediterranean outflow water, it was not possible to form waters of adequate density at 3200m, thus effectively shutting down abyssal flow along the Gardar Drift at Site 611.

Abyssal flow at the shallower Feni Drift site remained strong until 3.2 Ma and declined rapidly by about 2.5 Ma, corresponding to the beginnings of full-

scale Northern Hemisphere glaciation. The onset of Northern Hemisphere glaciation is also signaled by the large increase in the mass accumulation rate of continentally derived minerals in these North Atlantic sites.

To the extent that deep outflow waters exiting the North Atlantic are replaced by the surficial inflow of relatively warmer waters, the stepwise reduction in flow along the Gardar and Feni Drifts, beginning when the Mediterranean became closed to the North Atlantic, must be intimately associated with the late Cenozoic global cooling.

Acknowledgments

We wish to thank the ODP East Coast Repository at Lamont-Doherty Earth Observatory at Columbia University for providing the samples used in this study. We thank Joel Blum, Andrea Klaue and Marcus Johnson of the Michigan Radiogenic Isotope Geochemistry Laboratory for their assistance with the isotopic analyses. N. Hassold was supported by a fellowship from the Rackham Graduate School at the University of Michigan. A Turner Grant from the Department of Geological Sciences at the University of Michigan funded the radiogenic isotope analyses. We also thank Jan Bloemendal and an anonymous reviewer for providing helpful comments.

References

Berggren, W.A., Kent, D.V., Swisher, C.C.I., Aubry, M.-P., 1995. A revised Cenozoic geochronology and chronostratigraphy. In: Berggren, W.A., Kent, D.V., Hardenbol, J. (Eds.), Geochronology, Time Scales and Global Stratigraphic Correlations: A Unified Temporal Framework for an Historical Geology, Special Publication, vol. 52. Society of Economic Paleontologists and Mineralogists, pp. 129–212.

Billups, K., 2002. Late Miocene through early Pliocene deep water circulation and climate change viewed from the sub-Antarctic South Atlantic. Palaeogeography, Palaeoclimatology, Palaeoecology 185, 287–307.

Broecker, W.S., 1991. The great ocean conveyor. Oceanography 4, 79–89.

Cande, S.C., Kent, D.V., 1995. Revised calibration of the geomagnetic polarity timescale for the late Cretaceous and Cenozoic. Journal of Geophysical Research 100 (B4), 6093–6095.

Duggen, S., Hoernle, K., van den Bogaard, P., Rupke, L., Morgan, J.P., 2003. Deep roots of the Messinian salinity crisis. Nature 422, 602–606.

Ellwood, B.B., Ledbetter, M.T., 1977. Antarctic bottom water fluctuations in the Vema Channel: effects of velocity changes on particle alignment and size. Earth and Planetary Science Letters 35, 189–198.

Ellwood, B.B., Ledbetter, M.T., 1979. Paleocurrent indicators in deep-sea sediment. Science 203, 1335–1337.

Ellwood, B.B., Ledbetter, M.T., Johnson, D.A., 1979. Sedimentary fabric: a tool to delineate a high-velocity zone within a deep western Indian Ocean bottom current. Marine Geology 33, M51–M55.

Frank, M., Whiteley, N., Kasten, S., Hein, J.R., O'Nions, K., 2002. North Atlantic Deep Water export to the Southern Ocean over the past 14 Myr: evidence from Nd and Pb isotopes in ferromanganese crusts. Paleoceanography, 17. doi:10.1029/2000PA000606.

Gleason, J.D., Moore, T.C., Rea, D.K., Johnson, R.M., Owen, R.M., Blum, J.D., Hovan, S.A., Jones, C.E., 2002. Ichthyolith strontium isotope stratigraphy of a Neogene red clay sequence: calibrating eolian dust accumulation rates in the central North Pacific. Earth and Planetary Science Letters 202, 625–636.

Hailwood, E.A., Kidd, R.B., Dowling, L., 1987. The magnetic fabric of Neogene and Quaternary sediments on the Feni and Gardar Drifts, Northeastern Atlantic, Deep Sea Drilling Project Sites 610 and 611. In: Ruddiman, W.F., Kidd, R.B., Thomas, E., et al., Init. Repts. DSDP, vol. 94. U.S. Government Printing, Washington, pp. 1083–1089.

Hansen, B., Osterhus, S., Quadfasel, D., Turrell, W., 2004. Already the day after tomorrow? Science 305, 953–954.

Hovan, S.A., 1995. Late Cenozoic atmospheric circulation intensity and climatic history recorded by eolian deposition in the eastern Equatorial Pacific Ocean, Leg 138. In: Pisias, N.G., Mayer, L.A., Janecek, T.R., Palmer-Julson, A., van Andel, T.H.Proc. ODP, Sci. Results vol. 138. Ocean Drilling Program, College Station, TX, pp. 615–625.

Howe, J.A., Stoker, M.S., Stow, D.A.V., 1994. Late Cenozoic sediment drift complex, northeast Rockall Trough, North Atlantic. Paleoceanography 9, 989–999.

Hsü, K.J., Cita, M.B., Ryan, W.B.F., 1973. The origin of the Mediterranean evaporites. In: Ryan, W.B.F., Hsü, K.J., et al., Init Repts. DSDP, vol. 13. U.S. Government Printing, Washington, pp. 1203–1231.

Jansen, E., Raymo, M.E., 1996. Leg 162: new frontiers on past climates. In: Jansen, E., Raymo, M.E., Blum, P., et al., Proc. ODP, Init. Repts, vol. 162. Ocean Drilling Program, College Station, TX, pp. 5–20.

Joseph, L.H., Rea, D.K., van der Pluijm, B.A., 1998. Use of grain size and magnetic fabric analyses to distinguish among depositional environments. Paleoceanography 13, 491–501.

Joseph, L.H., Rea, D.K., van der Pluijm, B.A., Gleason, J.D., 2002. Antarctic environmental variability since the late Miocene: ODP Site 745, the East Kerguelen sediment drift. Earth and Planetary Science Letters 201, 127–142.

Joseph, L.H., Rea, D.K., van der Pluijm, B.A., 2004. Neogene history of the deep western boundary current at Rekohu Sediment Drift, Southwest Pacific (ODP Site 1124). Marine Geology 205, 185–206.

Kidd, R.B., Hill, P.R., 1987. Sedimentation on Feni and Gardar sediment drifts. In: Ruddiman, W.F., Kidd, R.B., Thomas, E., et al., (Eds.), Init. Repts. DSDP, vol. 94. U.S. Government Printing, Washington, pp. 1217–1244.

Krijgsman, W., Hilgen, F.J., Raffi, I., Sierro, F.J., Wilson, D.S., 1999. Chronology, causes and progression of the Messinian salinity crisis. Nature 400, 652–655.

Laberg, J.S., Dahlgren, K.I.T., Vorren, T.O., 2005. The Eocene–late Pliocene paleoenvironment in the Vøring Plateau area, Norwegian Sea—paleoceanographic implications. Marine Geology 214, 269–285.

Latouche, C., Maillet, N., Philipps, I., 1987. X-ray mineralogy of the clay fraction from Cenozoic strata, Leg 94: comparison with

previous North Atlantic data. In: Ruddiman, W.F, Kidd, R.B., Thomas, E., et al., Init. Repts. DSDP vol. 94. U.S. Government Printing Office, Washington, pp. 1089–1102.

Müller, G., Gastner, M., 1971. The 'Karbonate-Bombe', a simple device for the determination of the carbonate content in sediments, soils and other materials. Neues Jahrbuch fur Mineralogie 10, 466–469.

Murray, J.W., 1987. Benthic foraminifers and Neogene bottom-water masses at Deep Sea Drilling Project Leg 94 North Atlantic Sites. In: Ruddiman, W.F., Kidd, R.B., Thomas, E., et al., Init. Repts. DSDP, vol. 94. U.S. Government Printing, Washington, pp. 965–979.

Ravelo, A.C., Andreasen, D.H., 2000. Enhanced circulation during a warm period. Geophysical Research Letters 27, 1001–1004.

Raymo, M.E., Hodell, D., Jansen, E., 1992. Response of the deep ocean circulation to initiation of Northern Hemisphere glaciation (3–2 MA). Paleoceanography 7, 645–672.

Rea, D.K., Hovan, S.A., 1995. Grain size distribution and depositional processes of the mineral component of abyssal sediments: lessons from the North Pacific. Paleoceanography 10, 251–258.

Rea, D.K., Janecek, T.R., 1981. Mass-accumulation rates of the non-authigenic inorganic crystalline (eolian) component of deep-sea sediments from the western Mid-Pacific Mountains, Deep Sea Drilling Project Site 463. In: Thiede, J., Vallier, T.L., et al., (Eds.), Init, Rept., DSDP 62. U.S. Government Printing, Washington, pp. 653–659.

Rea, D.K., Hassold, N., Pares, J.M., van der Pluijm, B.A., 2003. Pliocene reduction in abyssal flow rates from analyses of drift deposits in the northern and southern oceans. Geological Society of America Abstracts with Program 35, 1193–1223.

Reid, J.L., 1979. On the contribution of the Mediterranean Sea outflow to the Norwegian–Greenland Sea. Deep-Sea Research 26A, 1199–1223.

Ruddiman, W.F., Kidd, R.B., Thomas, E., et al., 1987a. Site 610. Init. Repts. DSDP vol. 94. U.S. Government Printing Office, Washington, pp. 351–470.

Ruddiman, W.F., Kidd, R.B., Thomas, E., et al., 1987b. Site 611. Init. Repts. DSDP, vol. 94. U.S. Government Printing Office, Washington, pp. 471–590.

Seidenkrantz, M.S., Kouwenhoven, T.J., Jorissen, F.J., Shackleton, N.J., van der Zwaan, G.J., 2000. Benthic foraminifera as indicators of changing Mediterranean–Atlantic water exchange in the late Miocene. Marine Geology 163, 387–407.

Shipboard Scientific Party, 1998. Introduction. In: Keigwin, L.D., Rio, D., Acton, G.D., et al., (Eds.), Proc. ODP, Init. Repts. vol. 172. Ocean Drilling Program, College Station, TX, pp. 7–12.

St. John, K.K., Krissek, L.A., 2002. The late Miocene to Pleistocene ice—rafting history of southeast Greenland. Boreas 31, 28–35.

Takayama, T., Sato, T., 1987. Coccolith biostratigraphy of the North Atlantic Ocean, Deep Sea Drilling Project Leg 94. In: Ruddiman, W.F., Kidd, R.B., Thomas, E., et al., Init. Repts. DSDP vol. 94. U.S. Government Printing Office, Washington, pp. 651–694.

Tarling, D.H., Hrouda, F., 1993. The Magnetic Anisotropy of Rocks. Chapman and Hall, New York. 217 pp.

Thomas, E., 1987. Late Oligocene to Recent benthic foraminifers from Deep Sea Drilling Project Sites 608 and 610, northeastern North Atlantic. In: Ruddiman, W.F., Kidd, R.B., Thomas, E., et al., (Eds.), Init, Repts. DSDP, vol. 94. U.S. Government Printing, Washington, pp. 997–1015.

Wold, C.N., 1994. Cenozoic sediment accumulation on drifts in the northern North Atlantic. Paleoceanography 9, 917–941.

Wright, J.D., Miller, K.G., 1996. Control of North Atlantic Deep Water circulation by the Greenland–Scotland Ridge. Paleoceanography 11, 157–170.

Zhang, J., Scott, D.B., 1996. Integrated stratigraphy and paleoceanography of the Messinian (latest Miocene) across the North Atlantic Ocean. Marine Micropaleontology 26, 1–36.